

Optimal input reverberation and homeostatic self-organization towards the edge of synchronization

Sue L. Rhamidda,¹ Mauricio Girardi-Schappo,² and Osame Kinouchi¹

¹*Departamento de Física, FFCLRP, Universidade de São Paulo, Ribeirão Preto, SP, 14040-901, Brazil*

²*Departamento de Física, Universidade Federal de Santa Catarina, Florianópolis, SC, 88040-900, Brazil*

(*Electronic mail: suelam@usp.br, girardi.s@gmail.com, okinouchi@gmail.com)

(Dated: 21 May 2024)

Transient or partial synchronization can be used to do computations, although a fully synchronized network is sometimes related to the onset of epileptic seizures. Here, we propose a homeostatic mechanism that is capable of maintaining a neuronal network at the edge of a synchronization transition, thereby avoiding the harmful consequences of a fully synchronized network. We model neurons by maps since they are dynamically richer than integrate-and-fire models and more computationally efficient than conductance-based approaches. We first describe the synchronization phase transition of a dense network of neurons with different tonic spiking frequencies coupled by gap junctions. We show that at the transition critical point, inputs optimally reverberate through the network activity through transient synchronization. Then, we introduce a local homeostatic dynamic in the synaptic coupling and show that it produces a robust self-organization toward the edge of this phase transition. We discuss the potential biological consequences of this self-organization process, such as its relation to the Brain Criticality hypothesis, its input processing capacity, and how its malfunction could lead to pathological synchronization and the onset of seizure-like activity.

I. INTRODUCTION

Synchronization can be seen as the coincidence of spike times in a given population of interacting neurons¹. A consequence of synchronous spiking is the emergence of collective oscillations in the network. Transient synchronicity can be used for computation¹⁻³. However, a fully synchronous network – one in which the voltage oscillates with high amplitude and frequency – can be regarded as a seizure model^{4,5}. This pathological state could be the result of an intricate play of time scales⁶, and disruption of neuromodulation could generate some seizures by excessive excitation⁷. In this paper, we study a system with optimal input reverberation at the critical synchronization point. When subjected to a homeostatic mechanism, this dynamical framework could be used to understand some routes to the generation of seizure-like activity.

The Brain Criticality hypothesis states that the critical point is central to the processing of information in the healthy brain⁸⁻¹¹. Several studies show the presence of a critical state, with power-law-distributed neuronal avalanches and other scaling properties (for reviews, see¹²⁻¹⁵). The originally observed critical point was conjectured to separate an inactive state from a synchronous epileptic-like state⁸, although most of the theoretical works that followed relied on absorbing¹⁶ or Ising universality classes¹⁷ (a continuous phase transition between an inactive/disordered and an active/ordered state, where there is no synchronization). In such models, homeostatic mechanisms in synaptic coupling¹⁸, in firing gain¹⁹, or in multiple variables²⁰⁻²² lead to hovering around the critical point²³⁻²⁵.

The connection between power-law avalanches and a synchronization phase transition has also been investigated²⁶⁻²⁹. The authors used simplified models of phase oscillators²⁹, integrate-and-fire (IF) neurons^{28,30}, or abstract population

equations²⁷. However, the question remains whether the homeostatic dynamics could lead to the edge of synchronization, similarly to what happens with absorbing/Ising phase transitions.

Here, we introduce a network made up of map neurons under the influence of a simple rule of synaptic plasticity that is capable of pushing the system toward the edge of a synchronization phase transition. In particular, our map-based neurons offer a trade-off between analytical tractability, computational efficiency, and a rich repertoire of dynamical behaviors³³⁻³⁵. Unlike IF models, spikes appear naturally with a stereotyped waveform on maps as a consequence of the interplay between its time scales, yielding a dynamical picture

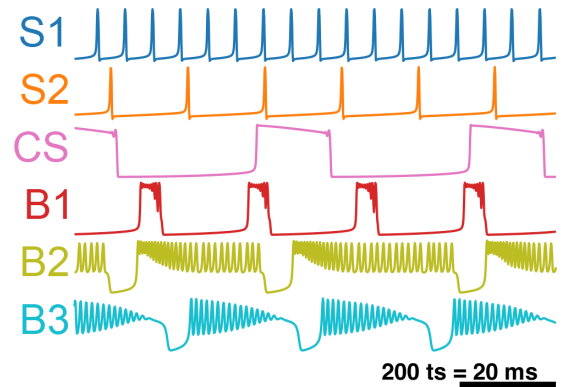


FIG. 1: Example attractors of the KTH neuron. Parameters: see Table S1 in the Supplementary Information. 10 time steps=1ms. The spikes are a result of the underlying interplay of fast (given by the T and K parameters; Eq. (1)) and slow time scales (δ_i and u parameters), analogously to what happens in conductance-based neuronal models. **S1, S2:** tonic spiking; **CS:** cardiac spiking; **B1, B2, B3:** dynamically distinct bursts.

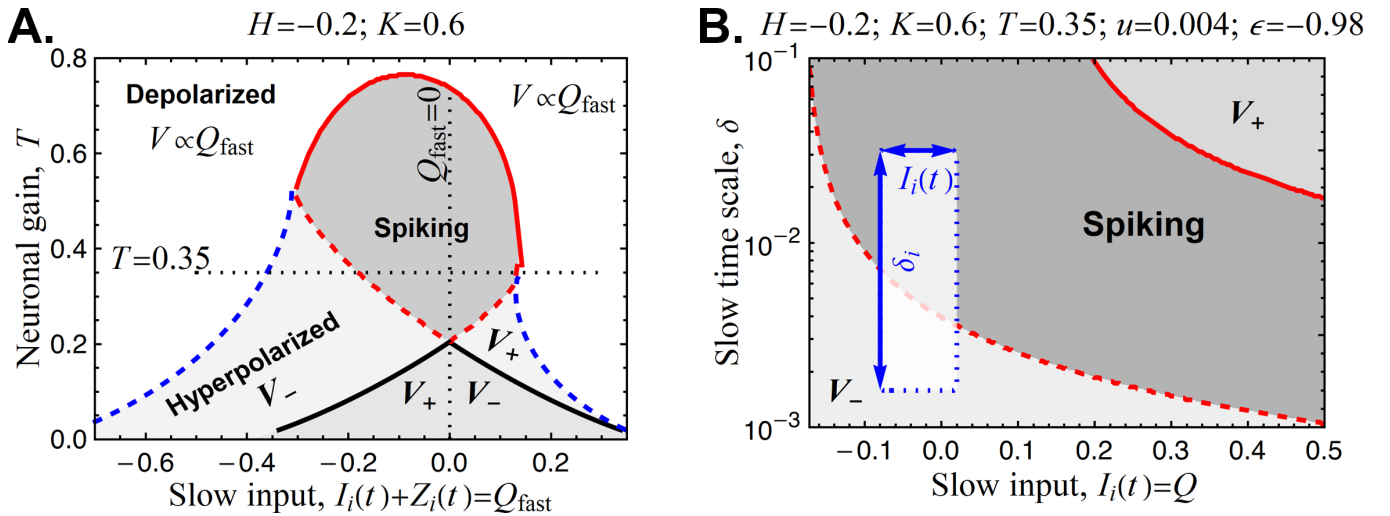


FIG. 2: Phase diagrams of an isolated neuron. V is the fixed point of the map, and V_+ and V_- are the hyperpolarized membrane potentials related to an upper ($V > 0$) and a lower ($V < 0$) stable fixed points. The *Spiking* phase has only stable limit cycles with periods that depend on Q , T , and δ . For both panels: (—) stable fold bifurcations of the upper (V_+) and lower (V_-) fixed points; (- - -) unstable fixed point fold bifurcation; (- - -) homoclinic bifurcation of limit cycle (infinite period bifurcation; stable fold point); (—) supercritical Neimark-Sacker bifurcation. **A.** Fast subsystem phase diagram obtained by replacing both the slow current $Z_i(t)$ and the input $I_i(t)$ with a constant field $Q_{\text{fast}} = Z_i(t) + I_i(t)$. For a fixed T , the $Z_i(t) + I_i(t)$ currents cause the state of the neuron to oscillate left and right in this graph. **B.** Phase diagram of the full neuron replacing only the input $I_i(t)$ with a constant field Q . The highlighted rectangle (height= 2Δ ; width= $I_i(t)$ amplitude) illustrates the state of a network of N neurons with uniformly distributed δ_i . The effect of the synaptic current is making a given neuron (with fixed δ_i) oscillate left and right within this rectangle. The amplitude of $I_i(t)$ has been exaggerated for visualization, since it is of the order of 10^{-4} (Fig. 3). The lines are the stability limits of the fixed point determined by the linear stability analysis described elsewhere^{31,32}.

that is generally similar to that of conductance-based models³². Contrary to previous similar maps^{31,32,36–38}, ours provides better control of the tonic spiking frequency – an important feature for the present study.

The synchronization phase transition we found has a power-law decay in the amplitude of the activity following stimuli due to critical slowing down. This yields optimal reverberation of the inputs. Some bifurcations with this feature are interpreted as second-order (critical) phase transitions in generalized Ising models^{39,40}.

We explore the role of the homeostasis parameters – henceforth called “hyperparameters” – and show that the convergence to the critical point is robust. This is because the system still reaches the vicinity of the critical point after either perturbing the synapses or changing the hyperparameters within a large range. The change in these homeostatic parameters implies only gross tuning for living systems. Our model provides a simple mechanistic explanation for two routes to the genesis of seizure-like activity: one is the disruption of the homeostatic dynamics and the second is the momentary synchrony due to external stimuli. Thus, such dynamics around the synchronization phase transition could have consequences for the maintenance of the healthy brain state (such as avoiding seizures⁷) and its processing of inputs¹.

II. RESULTS

First, we present a new neuron map model. Then, we examine its collective synchronization phase transition and show

that there is optimal reverberation of inputs at the critical point. Finally, we propose a synaptic mechanism that avoids synchronization, leading the network to lurk around the critical point vicinity. We then probe for its robustness and discuss how its disruption may trigger the onset of seizure-like activity via two different routes.

A. The map-based neuron model

The membrane potential $V_i(t)$ as function of time of an isolated neuron i is obtained by iterating the following equations:

$$\begin{aligned} V_i[t+1] &= \tanh\left(\frac{V_i[t] - KY_i[t] + Z_i[t] + I_i[t]}{T}\right), \\ Y_i[t+1] &= \tanh\left(\frac{V_i[t] + H}{T}\right), \\ Z_i[t+1] &= Z_i[t] - \delta_i Z_i[t] - u(V_i[t] - \varepsilon), \end{aligned} \quad (1)$$

where the t index denotes discrete time steps; K , T , H are parameters that control the fast dynamics; δ_i , u , ε control the slow variable $Z_i[t]$ ($\delta_i \ll 1$). The synaptic and external inputs enter in the current $I_i[t] = I_i^{\text{syn}}[t] + I_i^{\text{ext}}[t]$. A typical spike takes roughly 10 time steps, which then corresponds to 1 ms. We consider $I_i^{\text{ext}}[t] = 0$ unless otherwise specified.

This map was proposed in⁴¹ and called the KTH model, although its dynamic has not been described. The Y variable differs from previous models³⁵, making the fast subsystem more diverse. The membrane potential $V_i(t)$ is always bounded within $(-1, +1)$. This neuron can display fast and

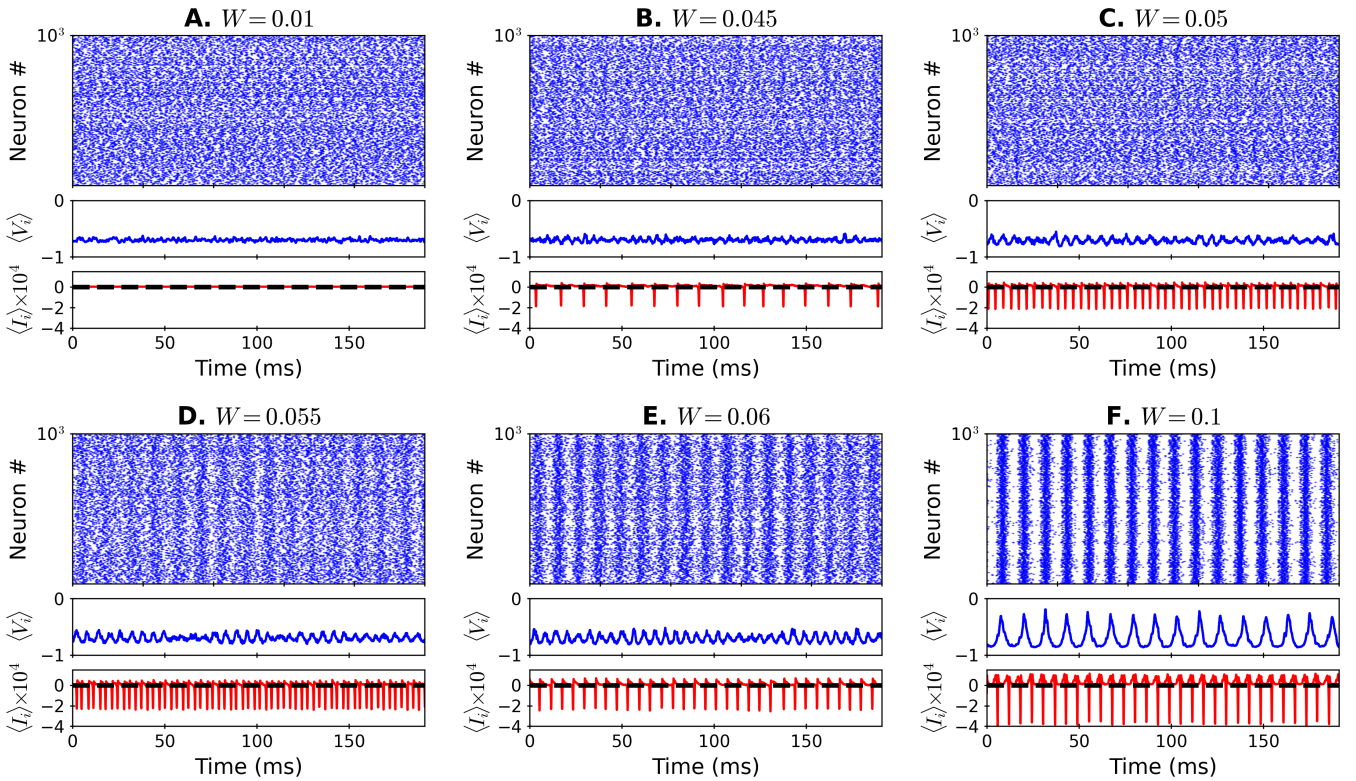


FIG. 3: Network activity as a function of W . All panels: raster plot showing spikes $S_i[t]$ (top); mean network potential (middle); and mean input $\langle I_i[t] \rangle \times 10^4$ (bottom). (---) mean over time, $\langle \langle I_i[t] \rangle \rangle_t$. Notice that the mean input is of the order 10^{-4} regardless of the coupling intensity. Parameters: $N = 1000$, $K = 0.6$, $T = 0.35$, $H = -0.2$, $\delta = 0.006$, $\Delta = 0.003$, $u = 0.004$, $\varepsilon = -0.98$.

slow spiking and bursting, and plateau spikes/bursts, with variable interspike and interburst intervals. It is similar to the Hindmarsh-Rose equations⁴². Some exemplars of the spiking behavior of a KTH neuron are shown in Fig. 1.

The parameters T and K modulate a fast self-coupling, and thus can be interpreted as a fast Sodium dynamics, since they are responsible for generating the spike depolarization. The slow Z_i current, on the other hand, is responsible for modulating the fast dynamics, and can be interpreted as a slow Potassium feedback with normalized inverse time constants δ_i and u and reversal potential ε .

We perform a slow-fast analysis of the map to unveil the bifurcations that lead to spiking, and consequently generate the synchronization phase transition to be studied ahead. It consists of substituting the slow variable by a fixed parameter, and tracing the bifurcation diagrams as a function of this new parameter – a procedure that is also known as *adiabatic approximation*³⁷. The bifurcations were identified via standard linear stability analysis (we followed the exact procedure described elsewhere³²).

To get a glimpse on the fast dynamics, we define the constant $Q_{\text{fast}} \equiv Z_i + I_i$ replacing both the Z_i current and the external input, and trace the bifurcation diagram in Fig. 2A. The spiking regime appears through an infinite-period (homoclinic) bifurcation or a supercritical Neimark-Sacker bifurcation, depending on the value of Q_{fast} . We also identified stable fold bifurcations that give rise to the coexistence of hyperpo-

larized states $V_+ > 0$ and $V_- < 0$ corresponding to stable fixed points. For a fixed T , the $Z_i(t) + I_i(t)$ currents cause the state of the neuron to oscillate left and right crossing the bifurcation lines and generating bursting (if $T \gtrsim 0.2$; *i.e.*, around the *bubble*) or cardiac spikes (via self-driven hysteretic cycles if $T \lesssim 0.2$; below the *bubble*).

We now replace only the external input with a constant parameter $Q \equiv I_i$ in order to understand the how the neurons will interact with one another when coupled in the network (Fig. 2B). In this case, the lower and upper fixed points, V_- and V_+ respectively, are separated by an intermediary spiking phase. For a fixed δ , the negatively hyperpolarized membrane, V_- , undergoes an infinite-period bifurcation as Q increases. In other words, if the neuron is sufficiently close to this bifurcation curve, then increasing external inputs are capable of generating both slow spiking (near the bifurcation) and fast spiking (away from the infinite-period bifurcation, but before crossing to the V_+ region). This is because the spiking frequency is known to have a power law divergence at the homoclinic bifurcation line^{32,43}. The proximity to the homoclinic bifurcation is behind the emergence of synchronization that we will study in the next sections.

B. The synchronization transition

All the results that follow were obtained for networks of coupled KTH maps. We build an all-to-all network of N neurons with diffusive coupling through gap junctions⁴⁴. The synaptic input on neuron $i = 1, \dots, N$ is:

$$I_i^{\text{syn}}[t] = \frac{W}{N} \sum_{j \neq i} (V_j[t] - V_i[t]), \quad (2)$$

W is the synaptic weight (assumed homogeneous for simplicity), and the sum runs over all the presynaptic neighbors j . We could have chosen to use heterogeneous coupling weights W_{ij} instead, as long as the weights obey a self-averaging distribution with mean $W = \langle W_{ij} \rangle$ taken over the off-diagonal pairs. In this case, the control parameter is still the mean synaptic weight W . Eq. (2) is a linearized Kuramoto interaction⁴⁵.

All parameters (except for δ_i) are homogeneous in the network. All neurons are set in a tonic spiking mode (exemplified in Fig. 1 with label S2). The parameter δ_i controls the recovery time scale of the slow variable $Z_i[t]$. Smaller δ_i 's imply in slower recovery times. Thus, this parameter is intrinsically related to the natural spiking frequency of each neuron. We force heterogeneity in the network by making each neuron i to have a unique δ_i uniformly chosen in the range $[\delta - \Delta; \delta + \Delta]$, $\langle \delta_i \rangle = \delta$. The resulting population is mixed in the sense that some neurons (with smaller δ_i) require more input than others (with larger δ_i) to cross the bifurcation line – see the highlighted rectangle in Fig. 2B representing a population of neurons. Thus, for $W = 0$, neurons are independent, but still fire regularly, yielding a non-vanishing global firing rate ρ (spikes per neuron in the stationary state). This suggests that a synchronization phase transition could occur for increasing $W > 0$ when a set of N neurons interact near the edge of this bifurcation.

A perfectly synchronized network has site-averaged membrane potential $\langle V_i[t] \rangle \equiv V[t]$ equal for all neurons, $V[t] = \langle V_i[t] \rangle = \langle V_j[t] \rangle$, making $\langle I_i[t] \rangle = 0$. However, the amplitude of the total synaptic input is proportional to W , which then determines whether a given neuron i enters or leaves the spiking region of the phase diagrams in Fig. 2. Thus, W is the control parameter for the synchronization transition.

We define an arbitrary threshold λ in order to obtain a binary spike variable $S_i[t]$, such that $S_i[t = t_{\text{spk}}] = 1$ if $V[t_{\text{spk}}] \geq \lambda$, then a spike occurred at $t = t_{\text{spk}}$; $S_i[t] = 0$ otherwise. The instantaneous firing rate of the network is defined as the fraction of spikes per unit of time, $\rho[t] = \langle S_i[t] \rangle = (1/N) \sum_i S_i[t]$.

Fig. 3 shows the activity as W is increased, suggesting that there is a synchronization critical point W_c . Note that the time-averaged input current $\langle \langle I_i[t] \rangle \rangle_t$ remains close to zero (of order 10^{-4}), although its amplitude increases allowing for neurons to spike together, as predicted. Collective oscillations with large amplitude (of order 1) emerge on the average potential $V[t]$ and consequently on the firing rate $\rho[t]$. The $\langle \dots \rangle_t$ represents the temporal average over a long time interval in the stationary state of the network.

Moreover, the raster plots show that neurons do not spike regularly within the synchronized state, making this a

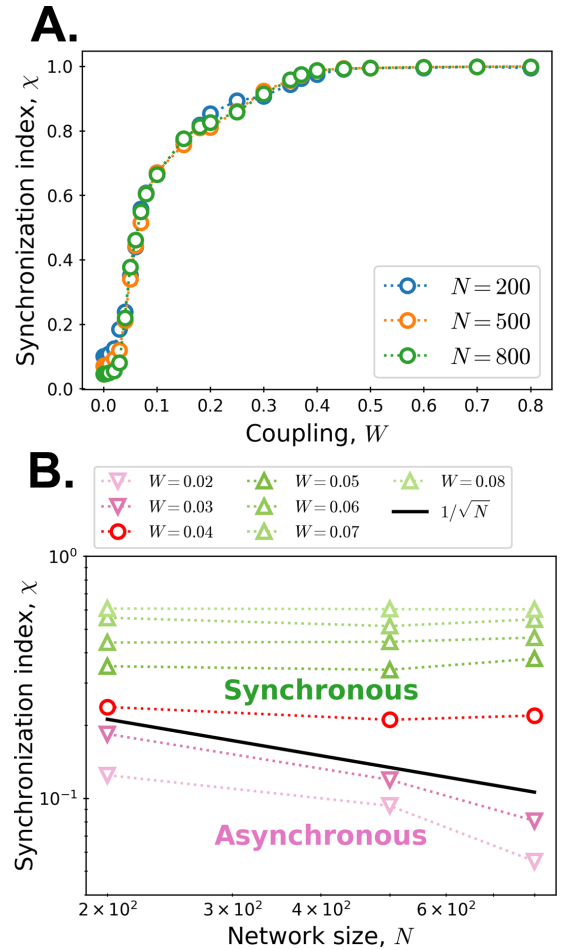


FIG. 4: Synchronization index as a function of coupling and network size. (A) χ rises as the network becomes synchronized with increasing W . (B) For $W \lesssim 0.04$, χ decays with the scaling $1/\sqrt{N}$ or faster, showing that the phase transition happens around $W_c \approx 0.04$, as expected. Due to the finite-size of the network, we consider the critical point to be in the range $0.04 \leq W_c \leq 0.05$. Parameters: $K = 0.6$, $T = 0.35$, $H = -0.2$, $\delta = 0.006$, $\Delta = 0.003$, $u = 0.004$ and $\varepsilon = -0.98$.

synchronous-irregular phase^{20,46} – see the interspike interval distribution for a single neuron in the network in Supplementary Fig. S1. Now, we characterize this phase transition by defining an order parameter, and then show that it optimizes the reverberation of inputs in the network.

C. Order parameter

We employ the synchronization index to identify the phase transition^{47,48}, since there is no vanishing activity – *i.e.*, absorbing state – near the transition point. The site-averaged network membrane potential is

$$\langle V_i[t] \rangle \equiv V[t] = \frac{1}{N} \sum_i V_i[t]. \quad (3)$$

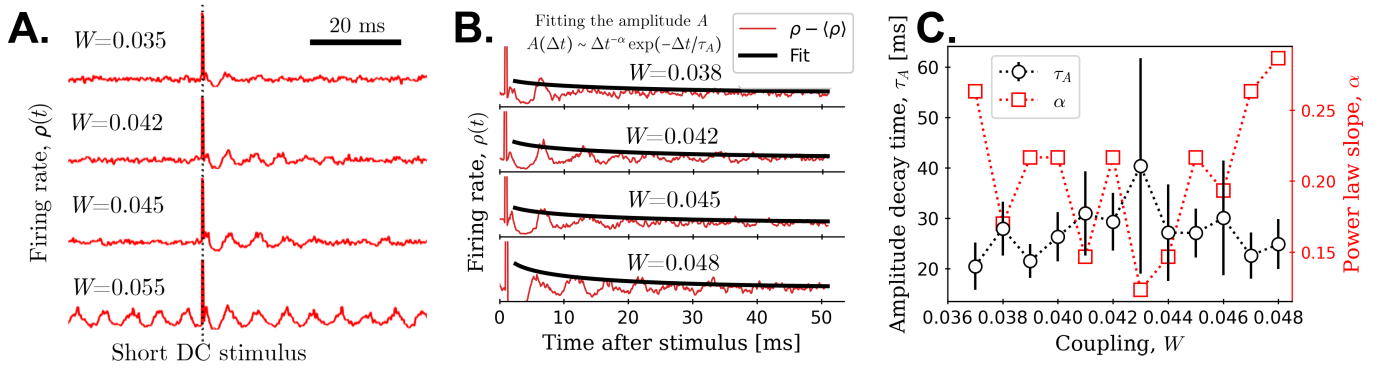


FIG. 5: Reverberating response to external stimuli near synchronization. **A.** Oscillations are damped for $W \lesssim 0.050$. For $W > 0.050$, the input only quickly perturbs the oscillation mode of the network. **B.** We estimated the characteristic time of the system by fitting the damping of the amplitude of the oscillations (see Supplementary Information for details). **C.** The characteristic time τ_A of the best fit has a maximum near the critical point due to critical slowing down. The shown α minimizes the fitting error of τ_A for each W ; it does not have error bars because it is a fixed parameter during the fitting procedure. τ_A is measured on the left-hand scale, and α is measured on the right-hand scale.

Making $\langle \dots \rangle_t$ the average over time in the stationary state, the temporal variance of the network voltage is:

$$\sigma_V^2 = \langle V[t]^2 \rangle_t - \langle V[t] \rangle_t^2, \quad (4)$$

whereas for a given neuron i in the network, we have:

$$\sigma_{V_i}^2 = \langle V_i[t]^2 \rangle_t - \langle V_i[t] \rangle_t^2, \quad (5)$$

leading to the synchronization index

$$\chi^2(N) = \frac{\sigma_V^2}{\langle \sigma_{V_i}^2 \rangle}. \quad (6)$$

The global variance is normalized by the average of the individual variances of the neurons. Thus, when $N \rightarrow \infty$, the index goes from $\chi \sim 1/\sqrt{N}$ in the asynchronous state to $\chi = 1$ for complete synchronization⁴⁸. This is because adding N temporally uncorrelated (or weakly correlated) signals results in a population average whose fluctuations have an amplitude of order $1/\sqrt{N}$.

There is a phase transition near $W = W_c \approx 0.045$ where incipient oscillations are forming. χ continuously grows with increasing coupling W , and the scaling $1/\sqrt{N}$ occurs for $W \lesssim 0.04$ (Fig. 4). Finite size effects prevent $\chi = 0$ even at $W \leq 0.04$, so in our simulations we consider that the critical point lies in the interval $0.04 \leq W_c \leq 0.05$, and estimate it to be $W_c = 0.045$.

D. Optimal input reverberation at criticality

We further characterize the phase transition by its response to external inputs near W_c . In the following, we show evidence that W_c optimizes the reverberation of the input through critical slowing down. We stimulate the network with a short square DC pulse input only after reaching the stationary state. The input is applied to 30% of the network and can be written as

$$I_i^{\text{ext}}[t] = I_0 \Theta[t - t_0] \equiv I_0 \Theta[\Delta t], \quad (7)$$

where $I_0 = 0.3$ is the amplitude and $\Theta[\Delta t]$ is a normalized square pulse (lasting ~ 1 ms), and $\Delta t = t - t_0$ is the delay after the stimulus is injected at t_0 . This forces a part of the network to spike together, momentarily synchronizing the few randomly selected neurons.

Fig. 5A shows the network activity $\rho[t]$ responding with damped oscillations both at the critical point W_c and in the subcritical state, $W < W_c$. Conversely, the synchronous state is only instantaneously perturbed, quickly returning to its previous persistent oscillation mode.

We define the reverberation of the input as the transient synchronization that appears after the stimulus stops³. The duration of the transient can be defined as the characteristic time for the damping of the amplitude A . Thus, we fitted the envelope of the oscillatory decay (Fig. 5B – for full details, see the Supplementary Information) using the function

$$A[\Delta t] \sim \Delta t^{-\alpha} \exp(\Delta t/\tau_A), \quad (8)$$

where τ_A is the damping characteristic time fitted using non-linear least squares; Δt is the delay after the stimulus (not to be confused with the Δ parameter); α is a critical exponent. We fit Eq. (8) for fixed α to obtain one τ_A for each α . We do this for many α and select the τ_A that minimizes the fitting error over α . See the Supplementary Figs. S2,S3 for details. We included the power-law term ($\Delta t^{-\alpha}$) inspired by two things. First, the typical amplitude decay in a supercritical Neimark-Sacker bifurcation as the critical point W_c is approached has the form $A \sim |W - W_c|^{-1/2}$. Secondly, we showed that the isolated KTH map presents supercritical Neimark-Sacker bifurcations in the slow-fast analysis. Eq. (8) also yielded less error when compared to a purely exponential fitting model, so we kept the power law.

The α and τ_A of the best fit are shown in Fig. 5C, yielding $\bar{\alpha} = 0.20 \pm 0.05$ (mean \pm SD over all best fits, see Supplementary Information). This temporal power-law decay of the activity is associated with critical slowing down in equilibrium phase transitions¹². The damping time is optimized at $W = 0.043$, close to W_c and within the critical range of the phase transition.

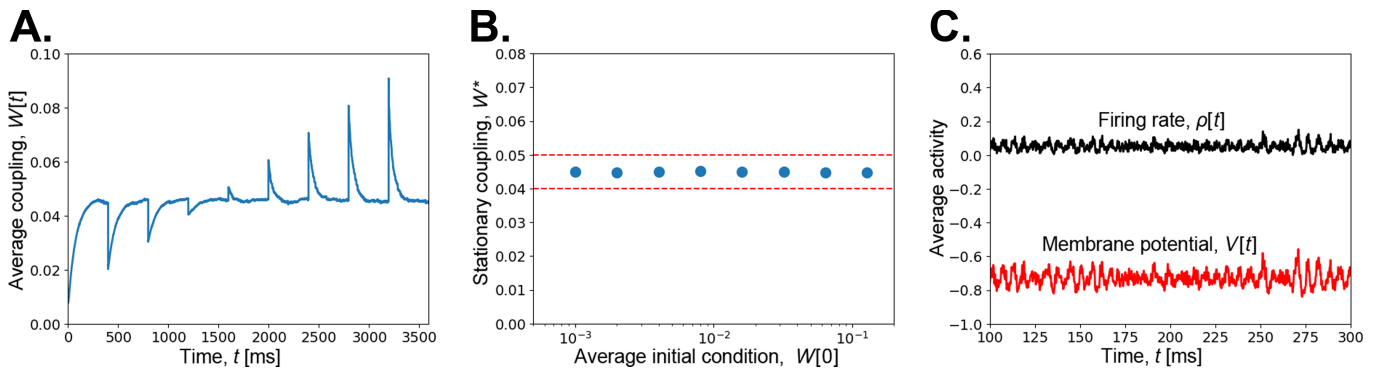


FIG. 6: Synchronization-avoiding homeostatic plasticity robustness. **A.** Average synaptic weight $W[t] = \langle W_{ij}[t] \rangle$ as a function of time. Synaptic weights converge to the stationary state $W^* \approx W_c = 0.45$ after perturbation. The network is periodically perturbed at every $t_p = 400n$ ms, $n = 1, \dots, 8$, artificially setting $W_{ij}[t_p] = 0.01(n+1)$. **B.** Stationary W^* versus various initial conditions $W[0] = \langle W_{ij}[t=0] \rangle$, $N = 200, A = 0.06, \tau = 1000, U_W = 0.1$. Dashed lines are guides for the eyes to locate the quasi-critical region where $W \in [0.04, 0.05]$. In this and in all the next figures the error bars are smaller than the symbols; **C.** Spontaneous activity $\rho[t]$ (black, upper) and average membrane potential $V[t]$ (red, lower) in the quasi-critical region: note the stochastic switching between large and small amplitude oscillations due to homeostatic hovering around the synchronization transition ($A = 0.058, W^* \approx 0.4, N = 200, \tau = 1000, U_W = 0.1$).

E. Synchronization-avoiding homeostatic plasticity

The input reverberation advantage at the critical point begs the question: Is there a mechanism that is capable of keeping the network functioning around the synchronization critical point? If so, what are the necessary ingredients for this dynamics without the need to fine-tune the synaptic couplings W_{ij} ?

We look for a dynamic that is capable of homeostatically going around a synchronization transition. Thus, if the network is synchronized, it must decrease the coincidence of spikes; otherwise, it should allow spikes to happen freely. Inspired by previous work^{19,22,49–51} (see Discussion), we then introduce the following anti-Hebbian plasticity:

$$W_{ij}[t+1] = W_{ij}[t] + \frac{1}{\tau} (A - W_{ij}[t]) - U_W W_{ij} S_i[t] S_j[t]. \quad (9)$$

This means that a synapse is depressed by a factor of $U_W W_{ij}$ whenever the pre- and postsynaptic spikes coincide, $S_i[t] S_j[t] = 1$. Otherwise, the weight W_{ij} is restored to the baseline synaptic coupling strength A on a time scale τ . Since synchronization increases spike coincidence, this mechanism is expected to avoid it. It also uses only local information to change synapses, since postsynaptic information $S_i[t]$ can be transmitted by retrograde dendritic spikes^{52,53}, similarly to what happens for spike-timing dependent plasticity⁵⁴.

For this part of the study, we cannot assume homogeneous weights beforehand. Thus, the initial couplings $W_{ij}[t=0]$ are chosen at random following a Gaussian distribution with mean over off-diagonal pairs $\langle W_{ij}[0] \rangle \neq W_c$. The variance of the initial distribution is not important, provided that all the $W_{ij}[0]$ are positive (excitatory). For each time step, the average synaptic weight is $W[t] = \langle W_{ij}[t] \rangle$. When reached, the steady state can be evaluated by taking $W^* = \langle \langle W_{ij} \rangle \rangle_t$ (first over off-diagonal pairs, then over time). Contrary to previous models, here the average synaptic coupling W^* depends on the pairwise site correlation, $\langle S_i S_j \rangle$. This means that the mechanism

we propose does not require an absorbing state to be able to drive the system towards the edge of the synchronization transition, thereby avoiding synchronization – see Discussion.

Recall that the synchronization phase transition starts at the critical point W_c , although the network is only fully synchronized when $\chi \sim 1$ for $W > W_c$. Thus, if our mechanism is capable of robustly converging to $W^* \sim W_c$ (avoiding W values where $\chi \sim 1$), we can safely say that it is successfully avoiding synchronization. Such an asymptotic limit ($W^* \sim W_c$) should be robust and depend only on the gross tuning of the hyperparameters (A, U_W, τ), regardless of initial conditions. We thus set out to investigate these features.

In Fig. 6, we can see that W^* converges to near W_c , within the quasicritical region $0.04 \leq W \leq 0.05$. This behavior is robust against temporal perturbations (Fig. 6A) and different initial conditions (Fig. 6B). The steady-state activity shows homeostatic oscillations similar to those typically observed in absorbing phase transition systems^{19,20}. However, here the system keeps switching between large and small amplitude oscillations (Fig. 6C). Additionally, Fig. 7A shows that the dynamics is robust both for small and large systems.

1. Dependence on the natural frequency dispersion Δ

Δ defines the broadness of the natural frequency distribution of neurons. The infinite-period bifurcation shown in the $\delta \times Q$ plane (Fig. 2) suggests that W_c (the synchronization point with constant W_{ij}) is a function of Δ . Larger Δ results in increased W_c . Introducing the homeostatic dynamics, we obtain growing W^* with increasing Δ (Fig. 7B). In other words, this means that the stationary state tracks the boundary of the phase transition, converging to the critical point W_c for each Δ . Note that all other parameters are fixed (A, τ, U_W and λ).

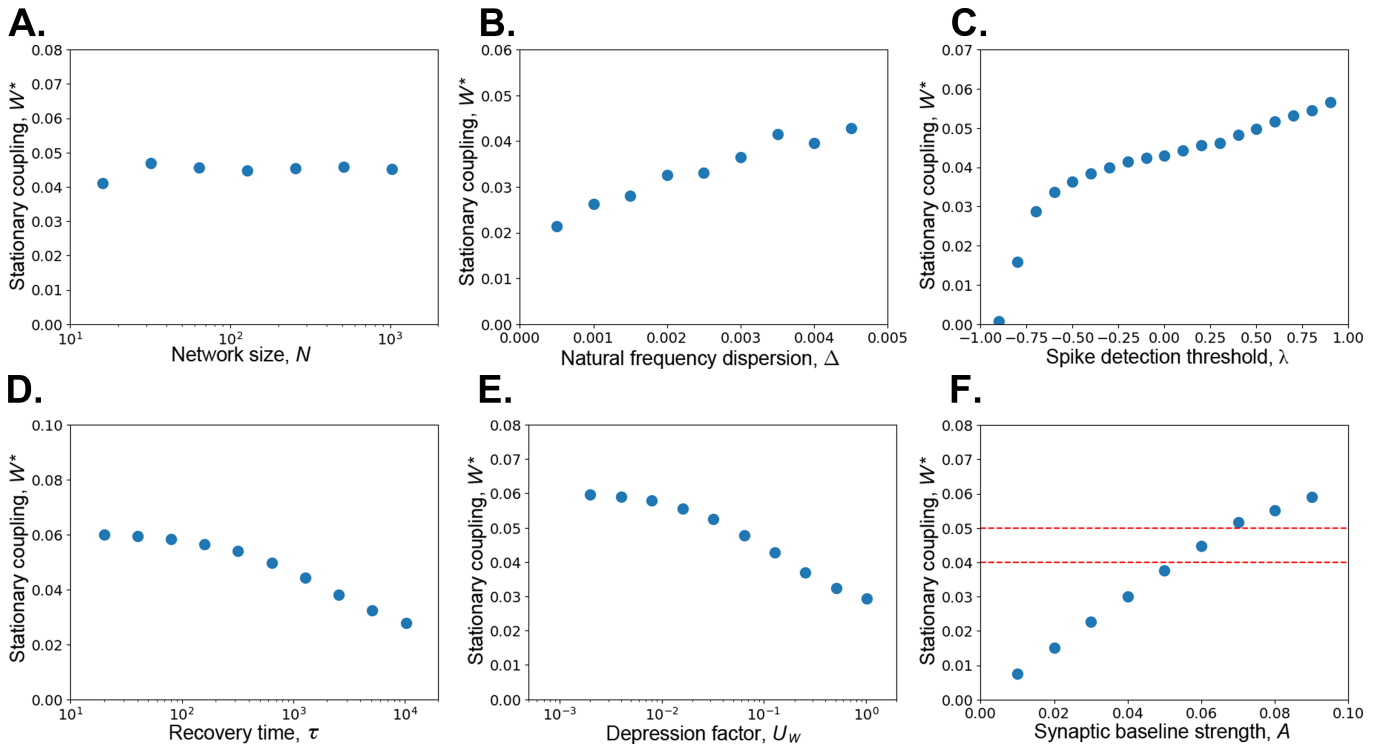


FIG. 7: Conditions for reaching the critical point. Each panel shows the behavior of the stationary state W^* as a function of a given parameter. All other parameters are kept fixed. **A.** The convergence to the critical point is robust for varying network size N . $A = 0.06$, $\tau = 1000$ and $U_W = 0.1$. **B.** The dynamics tracks the critical that shifts with Δ . $N = 200$, $A = 0.06$, $\tau = 1000$ and $U_W = 0.1$. **C.** The spike detection threshold λ has a convenient value (around zero), but is just a proxy for some underlying spike detection mechanism. $N = 200$, $A = 0.06$, $\tau = 1000$ and $U_W = 0.1$. **D.** The stationary state depends logarithmically on the depression recovery time τ . $N = 200$, $A = 0.06$ and $U_W = 0.1$. **E.** W^* also depends logarithmically on U_W . $N = 200$, $A = 0.06$ and $\tau = 1000$. **F.** The parameter A ultimately determines W^* and cannot be placed too far from W_c . $N = 200$, $\tau = 1000$ and $U_W = 0.1$. The dashed lines mark the critical region. The error bars are smaller than the symbols.

2. Effect of the spike detection threshold λ

The threshold λ defines the width of the spike that is effectively *perceived* by the depression term in W_{ij} . For a given neuron, a smaller λ implies in a longer time satisfying the condition $V_i[t] > \lambda$, yielding a longer depression. The value of λ is arbitrary, since we use it only as a simple way to define the coincidence between spikes. A possible biological mechanism that could implement the same detection is beyond the scope of our work.

There is a large interval $\lambda \in [-0.5; 0.5]$ where the stationary value W^* weakly depends on λ and goes to the phase transition range $W^* \in [0.04; 0.05]$ near $W_c \approx 0.045$ (Fig. 7C). We choose $\lambda = 0$ given the symmetry of the hyperbolic tangent that defines the membrane potential.

3. Dependence on hyperparameters

The synaptic recovery time τ controls the speed with which W^* returns to the baseline A in the absence of coincident spikes. This means that we have $W^* \approx A$ for small τ . For large τ , depression accumulates more quickly and makes W^* underestimate W_c in finite simulation times (Fig 7D). We hy-

pothesize that longer simulation times (of the order of many τ) could result in $W^* \sim W_c$ if δ_i are small enough leaving the neurons with very slow autonomous spiking. However, the asymptotic behavior of the stationary state is $W^* \sim -\log(\tau)$, which means that there is a wide range of τ that leads to the critical region around W_c .

The depression strength U_W controls the effect of coincident spikes on the synaptic couplings. U_W and τ could be replaced by a single parameter²², since both represent competing time scales. Therefore, the behavior of the stationary state as a function of U_W is equivalent to that as a function of τ . We have $W^* \approx A$ for small U_W , and large depression for large U_W (Fig 7E), underestimating W_c in a finite simulation time. Again, the asymptotic behavior of the system is $W^* \sim -\log(U_W)$, yielding a relatively long regime of near-criticality along the U_W range.

The hyperparameter that has the greatest effect is the synaptic baseline A . This is because without depression, the dynamic continually pushes the couplings toward A like a restoring force, resulting in $W^* = A$ exactly.

The depressing factor transforms this dynamic into sublinear with A (Fig. 7F). We cannot set A too far from W_c , otherwise the system would not converge to the critical point. Indeed, this has been known since the original introduction

of the depressing synapses¹⁸, and has been confirmed by a series of studies in systems with absorbing phase transitions^{19–22,49,50}. Such tuning is unavoidable for this type of homeostatic dynamics^{21,51} (see Discussion).

4. Input reverberation with homeostatic synchronization

Now that we have studied the properties of the input reverberation in networks without adaptation, and understood the role of hyperparameters in the synchronization dynamics, we can probe for the properties of the homeostatic networks.

These systems also show input reverberation (Fig. 8), mimicking the near-critical behavior of the static network with $W \approx W_c$. This is somewhat counterintuitive, since inputs create instantaneous synchrony, which in turn generates spike coincidence and strongly depresses synapses.

III. DISCUSSION

We introduced a map-based neuron with naturally occurring spikes and studied its bifurcations. Collectively adjusted in a tonic spiking mode and placed in an all-to-all network with diffusive couplings, these neurons synchronize through a continuous phase transition (defining a critical point W_c on the average coupling strengths).

The input reverberation duration is optimized at the transition point due to critical slowing down. We hypothesize that this could optimize information processing, since transient oscillations could be used for computations^{1,3}. In the subcritical region, synchrony is quickly lost and the network presents almost no transient oscillations. In the near-critical region and at the critical point, long transient oscillations appear after a perturbation (this is known as input reverberation) due to critical slowing down. The supercritical (synchronous) phase already has oscillations; and after the stimulus, the network quickly returns to this stationary state, yielding almost no transient dynamics. The reverberating input could work as a memory buffer for a much longer period of time than in the subcritical or supercritical cases.

Then, we proposed a self-organization mechanism that is capable of dynamically reaching the synchronization point and staying there. The mechanism was inspired by previous work, with the fundamental difference that here the synaptic depression is caused by the coincidence of pre and postsynaptic spikes. This generates homeostatic dynamics, leading the system to dwell close to the boundary of the synchronization phase transition. The resulting adaptive network has the following properties: a) an attractor (stationary) state W^* appears for the average coupling; b) this attractor is robust to temporal perturbations; c) there is a logarithmically large range of the hyperparameters in which W^* stays around the boundaries of the critical point W_c . Recently, a noisy homeostasis near a synchronization transition was proposed to model the sensitivity of the snake pit organ⁵⁵. Ideally, the baseline A should be near the critical point that leans toward the supercritical region. However, its precise value is not important

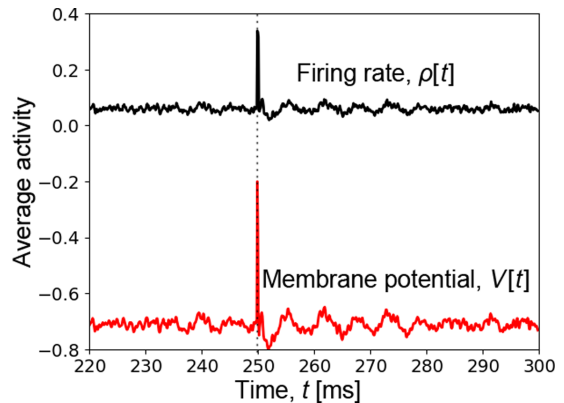


FIG. 8: Input reverberation on a homeostatic network with dynamical synapses. The transient oscillations are visible in the firing activity $\rho[t]$ (black, top) and in the average voltage $V[t]$ (red, bottom) after an stimulus of intensity $I_0 = 0.3$ (vertical dotted line). $A = 0.058$, $W^* \approx 0.045$, $N = 1000$, $\Delta = 0.003$, $\tau = 1000$ and $U_W = 0.1$.

since W^* also depends on the time scales τ and U_W . This feature also occurs in all systems that have similar types of adaptation^{18–22,50,51,56}.

In recent experiments^{57–59}, oscillatory transients similar to those in Fig. 6C (called “oscillatory bursts”) have been observed in M/EEG signals. We hypothesize that this could also be evidence of a synchronization-avoiding dynamics as proposed here, where the system homeostatically goes around a synchronization critical point. In absorbing systems with similar coupling dynamics, stochastic oscillations are driven by finite-size noise that perturbs a weakly stable focus^{19,60}. Here, the mechanism should be analogous, although the stable focus should be replaced by a stable spiral that is reminiscent of a limit cycle (that appears in the network for $W > W_c$).

A. Why map-based neurons?

The neuron model we used offers a compromise between the dynamical properties of conductance-based models, analytical tractability, and computational efficiency, showing a phenomenology analogous to the Hindmarsh-Rose model⁴². Maps offer a full framework for complex dynamics, from chaotic bursting to adaptable spiking threshold, to stochastic resonance^{32,35}. Furthermore, our map is richer than two dimensional systems like FitzHugh-Nagumo neurons and coupled Kaneko oscillators⁶¹.

Maps bring new insights and new challenges to the modeling of the synchronization phenomenon. Differently from the IF neurons, the spike in our map is not instantaneous; it is generated from the interplay between the K , T , δ_i and u time scales. It has all the spike phases that are traditionally observed in conductance-based models: up-rise and downfall, followed by a variable refractory period (after-hyperpolarizing potential), and it has no well-defined firing threshold, making the spike a continuous process. These features alone pose a big challenge to the modeling, since the

information in the network is neither instantaneously nor certainly transmitted through synaptic couplings. On the other hand, this allowed us to give an account of the necessary individual dynamics that can generate the collectively observed synchronization: here, the neurons need to have their slow recovery time scales (δ) distributed close to an infinite-period bifurcation.

The collective dynamics of map networks is not as trivially inferred from the microscopic details as in the case of IF networks (see, *e.g.*,⁶²). For example, power-law neuronal avalanches are easily observed in IF networks, since they are models of branching processes¹⁶ due to the instantaneous, and hence discrete, nature of the spike. Conversely, these avalanches require a delicate interplay between the synaptic and neuronal time scales in map-based neuronal networks; something that cannot be achieved with the simple tuning of a single parameter³⁸. Here, we took the time scale balance into account by choosing the values of T , K and H that give rise to the homoclinic bifurcation underlying the synchronization transition.

More complex models like ours are required to either confirm the universality hypothesis of the phase transitions that are predicted by simple models with stereotyped microscopic dynamics, such as the coupled Kuramoto oscillators; or to introduce new nonequilibrium universality classes⁶². We observed a critical exponent $\alpha = 0.20 \pm 0.05$ for the amplitude decay over time, pointing to a collective bifurcation different from the supercritical Neimark-Sacker. However, further studies are necessary to investigate the scaling law of the phase transition in our model, although this is beyond the scope of the current work.

B. To tune or not to tune

As nicely discussed by Hernandez-Urbina and Herrmann⁶³, the tuning of some parameters is unavoidable in the study of self-organization. Here, self-organization occurred because we turned the control parameter W into a slowly changing dynamical quantity via negative feedback from local information. This is enough to demonstrate the capacity of the system to reach the transition point autonomously, even though this will depend on the new set of parameters that controls the feedback (which we called the hyperparameters).

Due to homeostatic dynamics, there is a finite region in the hyperparameter space (τ , U_W , A) where the system is capable of autonomously reaching the synchronization point W_c . This region is relatively large, since W^* depends on $\log \tau$ and $\log U_W$. Regardless of the initial distribution of the synaptic weights $P(W_{ij}, t = 0)$, the weights self-organize into a stationary $P^*(W_{ij})$ with average W^* that can be as close to W_c as desired.

Such a tuning of the parameters that govern homeostasis happens even in the standard sandpile model⁶⁴. There, the accumulation and dissipation time scales have to be adjusted so that the excess of grains is controlled via feedback with the avalanching dynamics.

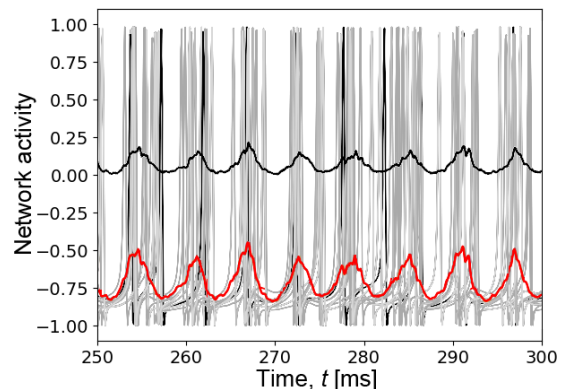


FIG. 9: Synchronous seizure-like activity due to impaired homeostasis. Example of the homeostatic network activity with an impaired combination of homeostatic parameters. In this case, the stationary state W^* converges to the supercritical synchronous state. Average voltage $V = \langle V_i \rangle$ (red oscillations, bottom); average activity $\rho = \langle S_i \rangle$ (black oscillations above zero). Background: spikes of a few neurons selected at random. $N = 1000$, $W^* \approx 0.064$, $A = 0.1$, $\tau = 1000$, $U_W = 0.1$.

C. The absorbing state is not necessary for the Synchronization-Avoiding Self-Organization (SASO)

Several homeostatic mechanisms have been proposed to self-organize a network to criticality; for a review, see²³. They are based on the same principle: If the network has small activity $\rho \sim 0$ (*i.e.*, if the system is in the absorbing phase $W < W_c$, and is subcritical), then W must slowly grow towards W_c ; or else if the network activity is too large $\rho \approx 1$ (the system is in the active phase, $W > W_c$, and is supercritical), then W must decrease towards W_c . The same can be accomplished with parameters other than synaptic coupling²³. This mechanism is asymptotically present even in the Sandpile model⁶⁴ – the seminal model for Self-Organized Criticality (SOC)⁶⁵. In the context of neural networks, it was introduced by Levina, Herrmann, and Geisel¹⁸ through short-term synaptic depression and recovery. As a consequence, the activity of the network displays stochastic homeostatic oscillations around the critical point^{23,56}.

SOC and its sister mechanisms (such as Self-Organized quasi-Criticality – SOqC, Self-Organized Bistability – SOB, and Self-Organized Collective Oscillations – SOCO) are theoretically interpreted via stochastic Langevin equations for the firing rate ρ coupled to an average adaptive synaptic field W ²⁵. A common feature connecting the dynamics of all these theories is that the phase transition must occur towards an absorbing state where the firing rate is $\rho = 0$. The reason is simple: the microscopic dynamics that give rise to these theories have a synaptic depression term of the form $-U_W W_{ij} S_j$, where $S_j = 1$ when a presynaptic spike happens (zero otherwise) and $U_W > 0$ is an arbitrary constant^{23,25}; W_{ij} is the synaptic coupling conductance. Thus, the averaged synaptic coupling field is depressed proportionally to the firing rate, since $U_W \langle W_{ij} S_j \rangle = U_W W \rho$, and the depression turns off whenever $\rho = 0$ allowing the synaptic coupling to be restored.

In contrast, the microscopic mechanism we proposed in Eq. (9) depends on the coincidence of pre- and postsynaptic spikes, which gives rise to an average adaptive synaptic field that is depressed proportionally to the pairwise site correlation, since $U_W \langle W_{ij} S_i S_j \rangle = U_W W \langle S_i S_j \rangle$. The recovery of the average synaptic field starts only when $\langle S_i S_j \rangle = 0$, which is directly related to a null synchronization index $\chi = 0$. This is because χ^2 is the variance of the network relative to the individual membrane potentials. Notwithstanding, χ is our order parameter of choice. We name this mechanism by Synchronization-Avoiding Self-Organization, or SASO, and it works even in the absence of an absorbing state. In other words, the system may have non-vanishing firing rate in both sides of the critical point W_c , and synchronization will still be prevented if the conditions that we unveiled for the hyperparameters are obeyed.

D. Relevance to epilepsy

Epilepsy is a complex phenomenon that depends on multiple factors⁶⁶. Its expression depends on both the structural⁶⁷ and the dynamical⁶⁸ features. In the early observation of neuronal avalanches, seizures were hypothesized to correspond to a supercritical state with synchronized spikes and oscillations at the average population voltage⁸. Other authors have also suggested that epilepsy is related to loss of criticality^{69–71}, but no mechanism has been proposed. A synchronization transition can be used as a simple model for epileptic seizures^{5,66}. In this context, there are some attempts to model the transition into ictal activity (*e.g.*, fast oscillations with large amplitude) both at the population⁵ and at the electroencephalography⁶ levels. However, only qualitative comparisons have been made between self-organized critical models and empirical data⁶⁹. Thus, considering the similarities between the dynamics in our model and the synchronization feature of seizure-like activity observed experimentally^{72–74}, we study the transition to synchronization as a theoretical approximation of the onset of seizure-like activity.

Some authors suggest that the ictal state may be elicited by increased excitation resulting from an underlying neuromodulatory process⁷. In our model, this is captured by combining the parameters of synaptic depression in such a way that $W^* \approx A$, disrupting the near-criticality homeostatic balance, and driving the system towards supercritical synchronized oscillations. Namely, considering $A > W_c$ some malfunction could produce a combination of the recovery time τ and depression factor U_W that is incapable of suppressing W^* sufficiently from the baseline A . This would keep the network hyperexcited, favoring synchronization and generating fast and large waves (Fig. 9). An analogous transition is achieved by an intricate interplay of slow-fast time scales in another phenomenological model for the EEG activity of the brain⁶.

Reflex seizures can also be triggered by external stimuli that statistically favor synchrony^{75–77}. This is also captured by our model: Being on the verge of the synchronization phase transition, our network is capable of reverberating synchrony-provoking stimuli over long times (Fig. 8). Although this

could sometimes be advantageous to computation^{1,2}, a faulty configuration of neuronal and synaptic time scales (governed by T , δ_i , K , τ and U_W) could also excessively delay the damping of the response oscillations beyond the optimal τ_A value. Consequently, the loss of damping would turn the input reverberation into sustained supercritical synchronized oscillations, triggering seizure-like activity.

E. Other attempts to suppress synchronization

Some studies have looked at the influence of synaptic plasticity on synchronization⁷⁸, or found first order synchronization transitions in map-based networks⁷⁹. A theory has also been recently proposed⁸⁰ to describe Hebbian and anti-Hebbian synaptic adaptation in Sompolinsky *et al.*⁸¹-like rate networks. Here, we proposed a simulation of a spiking neural networks that can be explained under the umbrella of the SOC-derived theories²⁵, where the adaptive field receives feedback from the pairwise site correlation to avoid synchronization. Others have developed a global mechanism that can be used to control the synchronization near a Hopf bifurcation⁸². Controlling or even suppressing synchronization is a timely subject, given that oscillations are ubiquitously found both in nature and in many engineering applications.

In the context of the brain, synchronization-suppressing control feedback could be used to extinguish pathological oscillations. The method consists in adding a direct feedback of the average membrane potential onto itself after a given delay⁸². The method was successfully applied to mean-field networks of Hindmarsh-Rose and Rulkov neurons. This strategy was also successful in eliminating the synchronization of hierarchically clustered complex networks of bursting Rulkov maps coupled by different types of synapses^{83–85}.

The main difference is that ours is a local mechanism, since it involves only the pre- and postsynaptic spikes. Not only that, but in the feedback control theory, the feedback weight that couples the global average membrane potential to each neuron is constant. Conversely, in our mechanism the coupling constant is itself adaptive, and it depends only on local information. Our mechanism is not intended to be used as a form of externally controlling the synchronization. Rather, we hypothesize that it could be an intrinsic mechanism built-in to the network in order to avoid pathological synchronization.

IV. PERSPECTIVES

The simplified dense topology allowed us to isolate the effects of the dynamics on the synchronization. Therefore, the effect of connectivity is not yet explored. Our model can also be expanded by considering chemical synapses and excitatory and inhibitory populations of neurons. The role of synaptic noise in the system and how to regulate the hyperparameters of the homeostasis are also open questions.

Our findings not only contribute to the broader understanding of brain criticality, but also present innovative perspectives on the role of synchronization phase transitions and critical

slowing down in brain information processing. The proposed homeostatic synaptic dynamics adds a novel dimension to the exploration of network behavior near bifurcation points and yields simplified (yet general) explanations for neurological disorders.

SUPPLEMENTARY MATERIAL

We provide extra figures and information about the microscopic activity of the network and the fitting of the damping characteristic time.

ACKNOWLEDGMENTS

S.L.R. acknowledges a CAPES Ph.D. fellowship. O.K. acknowledges CNAIPS-USP, FAPESP support, and a CNPq research fellowship. S.L.R. and O.K. thank the CEPID NEUROMAT support. The authors are grateful for advice from Mauro Copelli and Antônio C. Roque.

AUTHOR DECLARATIONS

Conflict of Interest

The authors have no conflicts to disclose.

Author Contributions

S.L.R.: Conceptualization (equal); Investigation (equal); Validation (equal); Visualization (equal); Writing the original draft (equal). M.G.-S.: Investigation (equal); Validation (equal); Supervision (equal); Visualization (equal); Writing (equal). O.K.: Conceptualization (equal); Investigation (equal); Supervision (equal); Validation (equal); Writing original draft (equal).

DATA AVAILABILITY STATEMENT

The data that support the findings of this study are available within the article and its supplementary material.

REFERENCES

- ¹R. Brette, “Computing with neural synchrony,” *PLoS Comput Biol* **8**, e1002561 (2012).
- ²E. M. Izhikevich, “Polychronization: Computation with Spikes,” *Neural Comput.* **18**, 245–282 (2006).
- ³A. Palmigiano, T. Geisel, F. Wolf, and D. Battaglia, “Flexible information routing by transient synchrony,” *Nat Neurosci.* **20**, 1014–1022 (2017).
- ⁴K. Lehnertz, S. Bialonski, M.-T. Horstmann, D. Krug, A. Rothkegel, M. Staniek, and T. Wagner, “Synchronization phenomena in human epileptic brain networks,” *J Neurosci Methods.* **183**, 42–48 (2009).
- ⁵S. Rich, A. Hutt, F. K. Skinner, T. A. Valiante, and J. Lefebvre, “Neurostimulation stabilizes spiking neural networks by disrupting seizure-like oscillatory transitions,” *Sci Rep* **10**, 15408 (2020).
- ⁶V. K. Jirsa, W. C. Stacey, P. P. Quilichini, A. I. Ivanov, and C. Bernard, “On the nature of seizure dynamics,” *Brain* **137**, 2210–2230 (2014).
- ⁷F. Lopes da Silva, W. Blanes, S. N. Kalitzin, J. Parra, P. Suffczynski, and D. N. Velis, “Epilepsies as dynamical diseases of brain systems: basic models of the transition between normal and epileptic activity,” *Epilepsia* **44 Suppl 12**, 72–83 (2003).
- ⁸J. M. Beggs and D. Plenz, “Neuronal avalanches in neocortical circuits,” *J. Neurosci.* **23**, 11167–11177 (2003).
- ⁹O. Kinouchi and M. Copelli, “Optimal dynamical range of excitable networks at criticality,” *Nat. Phys.* **2**, 348–351 (2006).
- ¹⁰J. M. Beggs, “The criticality hypothesis: how local cortical networks might optimize information processing,” *Philos. Trans. R. Soc. A* **366**, 329–343 (2008).
- ¹¹W. L. Shew and D. Plenz, “The functional benefits of criticality in the cortex,” *Neuroscientist* **19**, 88–100 (2013).
- ¹²L. Cocchi, L. L. Gollo, A. Zalesky, and M. Breakspear, “Criticality in the brain: A synthesis of neurobiology, models and cognition,” *Prog. Neurobiol.* **158**, 132–152 (2017).
- ¹³M. Girardi-Schappo, “Brain criticality beyond avalanches: open problems and how to approach them,” *J Phys Complex* **2**, 031003 (2021).
- ¹⁴D. Plenz, T. L. Ribeiro, S. R. Miller, P. A. Kells, A. Vakili, and E. L. Capek, “Self-organized criticality in the brain,” *Front. Phys.* **9**, 639389 (2021).
- ¹⁵J. O’Byrne and K. Jerbi, “How critical is brain criticality?” *Trends Neurosci.* **45**, P820–837 (2022).
- ¹⁶T. T. A. Carvalho, A. J. Fontenele, M. Girardi-Schappo, T. Feliciano, L. A. A. Aguiar, T. P. L. Silva, N. A. P. de Vasconcelos, P. V. Carelli, and M. Copelli, “Subsampled directed-percolation models explain scaling relations experimentally observed in the brain,” *Front. Neural Circuits* **14**, 83 (2021).
- ¹⁷A. Ponce-Alvarez, A. Jouary, M. Privat, G. Deco, and G. Sumbre, “Whole-brain neuronal activity displays crackling noise dynamics,” *Neuron* **100**, 1446–1459.e6 (2018).
- ¹⁸A. Levina, J. M. Herrmann, and T. Geisel, “Dynamical synapses causing self-organized criticality in neural networks,” *Nat. Phys.* **3**, 857–860 (2007).
- ¹⁹O. Kinouchi, L. Brochini, A. A. Costa, C. J. G. F., and M. Copelli, “Stochastic oscillations and dragon king avalanches in self-organized quasi-critical systems,” *Sci. Rep.* **9**, 3874 (2019).
- ²⁰M. Girardi-Schappo, B. L. A. A. Costa, T. T. A. Carvalho, and O. Kinouchi, “Synaptic balance due to homeostatically self-organized quasi-critical dynamics,” *Phys. Rev. Res.* **2**, 012042 (2020).
- ²¹M. Girardi-Schappo, E. F. Galera, T. T. Carvalho, L. Brochini, N. L. Kamiji, A. C. Roque, and O. Kinouchi, “A unified theory of E/I synaptic balance, quasicritical neuronal avalanches and asynchronous irregular spiking,” *J. Phys. Complex.* **2** (2021), 10.1088/2632-072X/ac2792.
- ²²G. Menesse, B. Marin, M. Girardi-Schappo, and O. Kinouchi, “Homeostatic criticality in neuronal networks,” *Chaos Solitons Fractals* **156**, 111877 (2022).
- ²³O. Kinouchi, R. Pazzini, and M. Copelli, “Mechanisms of self-organized quasicriticality in neuronal networks models,” *Front. Phys.* **8**, 583213 (2020).
- ²⁴D. R. Chialvo, S. A. Cannas, T. S. Grigera, D. A. Martin, and D. Plenz, “Controlling a complex system near its critical point via temporal correlations,” *Sci. Rep.* **10**, 12145 (2020).
- ²⁵V. Buendia, S. di Santo, J. A. Bonachela, and M. A. Muñoz, “Feedback mechanisms for self-organization to the edge of a phase transition,” *Front. Phys.* **8**, 333 (2020).
- ²⁶S.-S. Poil, R. Hardstone, H. D. Mansvelder, and K. Linkenkaer-Hansen, “Critical-state dynamics of avalanches and oscillations jointly emerge from balanced excitation/inhibition in neuronal networks,” *J. Neurosci.* **32**, 9817–9823 (2012).
- ²⁷S. Di Santo, P. Villegas, R. Burioni, and M. A. Muñoz, “Landau-ginzburg theory of cortex dynamics: Scale-free avalanches emerge at the edge of synchronization,” *Proc Natl Acad Sci USA* **115**, E1356–E1365 (2018).
- ²⁸L. Dalla Porta and M. Copelli, “Modeling neuronal avalanches and long-range temporal correlations at the emergence of collective oscillations: Continuously varying exponents mimic M/EEG results,” *PLoS Comput. Biol.* **15**, e1006924 (2019).

- ²⁹V. Buendía, P. Villegas, R. Burioni, and M. A. Muñoz, “Hybrid-type synchronization transitions: Where incipient oscillations, scale-free avalanches, and bistability live together,” *Phys. Rev. Res.* **3**, 023224 (2021).
- ³⁰S.-S. Poil, A. van Ooyen, and K. Linkenkaer-Hansen, “Avalanche dynamics of human brain oscillations: relation to critical branching processes and temporal correlations,” *Hum. Brain Mapp.* **29**, 770–777 (2008).
- ³¹O. Kinouchi and M. H. R. Tragtenberg, “Modeling neurons by simple maps,” *Int J Bifurcat Chaos* **6**, 2343–2360 (1996).
- ³²M. Girardi-Schappo, G. S. Bortolotto, R. V. Stenzinger, J. J. Gonsalves, and M. H. Tragtenberg, “Phase diagrams and dynamics of a computationally efficient map-based neuron model,” *PLoS One* **12**, e0174621 (2017).
- ³³M. Courbage and V. I. Nekorkin, “Map-based models in neurodynamics,” *Int J Bifurcat Chaos* **20**, 1631–1651 (2010).
- ³⁴B. Ibarz, J. M. Casado, and M. A. F. Sanjuán, “Map-based models in neuronal dynamics,” *Phys. Rep.* **501**, 1–74 (2011).
- ³⁵M. Girardi-Schappo, M. Tragtenberg, and O. Kinouchi, “A brief history of excitable map-based neurons and neural networks,” *J. Neurosci. Methods* **220**, 116–130 (2013).
- ³⁶S. M. Kuva, G. F. Lima, O. Kinouchi, M. H. Tragtenberg, and A. C. Roque, “A minimal model for excitable and bursting elements,” *Neurocomputing* **38-40**, 255–261 (2001).
- ³⁷M. Copelli, M. Tragtenberg, and O. Kinouchi, “Stability diagrams for bursting neurons modeled by three-variable maps,” *Physica A* **342**, 263–269 (2004).
- ³⁸M. Girardi-Schappo, O. Kinouchi, and M. H. R. Tragtenberg, “Critical avalanches and subsampling in map-based neural networks coupled with noisy synapses,” *Phys. Rev. E* **88**, 024701 (2013).
- ³⁹C. S. O. Yokoi, M. J. de Oliveira, and S. R. Salinas, “Strange attractor in the Ising model with competing interactions on the Cayley tree,” *Phys. Rev. Lett.* **54(3)**, 163–166 (1985).
- ⁴⁰M. H. R. Tragtenberg and C. S. O. Yokoi, “Field behavior of an Ising model with competing interactions on the Bethe lattice,” *Phys. Rev. E* **52(3)**, 2187–2197 (1995).
- ⁴¹O. Kinouchi, “Extended dynamical range as a collective property of excitable cells,” arXiv:cond-mat/0108404 [cond-mat.dis-nn] (2001), 10.48550/arXiv.cond-mat/0108404.
- ⁴²J. L. Hindmarsh and R. Rose, “A model of neuronal bursting using three coupled first order differential equations,” *Proc R Soc Lond B Biol Sci.* **221**, 87–102 (1984).
- ⁴³S. H. Strogatz, *Nonlinear Dynamics and Chaos: With Applications to Physics, Biology, Chemistry, and Engineering* (Westview Press, 2001).
- ⁴⁴A. Roth and M. C. W. van Rossum, “Modeling synapses,” in *Computational Modeling Methods for Neuroscientists*, edited by E. de Schutter (The MIT Press, Cambridge, MA, USA, 2010).
- ⁴⁵Y. Kuramoto, *Chemical Oscillations, Waves, and Turbulence*, Vol. 19 (Springer Berlin Heidelberg, 1984).
- ⁴⁶N. Brunel, “Dynamics of sparsely connected networks of excitatory and inhibitory spiking neurons,” *J. Comput. Neurosci.* **8**, 183–208 (2000).
- ⁴⁷D. Golomb and J. Rinzel, “Clustering in globally coupled inhibitory neurons,” *Physica D* **72**, 259–282 (1994).
- ⁴⁸D. Golomb, “Neuronal synchrony measures,” *Scholarpedia* **2**, 1347 (2007), revision #128277.
- ⁴⁹L. Brochini, A. A. Costa, M. Abadi, A. C. Roque, J. Stolfi, and O. Kinouchi, “Phase transitions and self-organized criticality in networks of stochastic spiking neurons,” *Sci. Rep.* **6**, 35831 (2016).
- ⁵⁰A. A. Costa, M. J. Amon, O. Sporns, and L. H. Favela, “Fractal analyses of networks of integrate-and-fire stochastic spiking neurons,” in *International Workshop on Complex Networks* (Springer, 2018) pp. 161–171.
- ⁵¹G. Menesse and O. Kinouchi, “Less is different: Why sparse networks with inhibition differ from complete graphs,” *Phys. Rev. E* **108**, 024315 (2023).
- ⁵²K. Holthoff, Y. Kovalchuk, and A. Konnerth, “Dendritic spikes and activity-dependent synaptic plasticity,” *Cell Tissue Res* **326**, 369–377 (2006).
- ⁵³L. L. Gollo, O. Kinouchi, and M. Copelli, “Active dendrites enhance neuronal dynamic range,” *PLoS Comput. Biol.* **5**, e1000402 (2009).
- ⁵⁴R. O. Shimoura, R. F. O. Pena, V. Lima, N. L. Kamiji, M. Girardi-Schappo, and A. C. Roque, “Building a model of the brain: from detailed connectivity maps to network organization,” *Eur Phys J Spec Top* **230**, 2887–2909 (2021).
- ⁵⁵I. R. Graf and B. B. Machta, “A bifurcation integrates information from many noisy ion channels and allows for milli-kelvin thermal sensitivity in the snake pit organ,” *Proc. Natl. Acad. Sci. USA* **121**, e2308215121 (2024).
- ⁵⁶J. A. Bonachela, S. de Franciscis, J. J. Torres, and M. A. Muñoz, “Self-organization without conservation: are neuronal avalanches generically critical?” *J. Stat. Mech.* **2010**, P02015 (2010).
- ⁵⁷F. van Ede, A. J. Quinn, M. W. Woolrich, and A. C. Nobre, “Neural oscillations: Sustained rhythms or transient burst-events?” *Trends Neurosci.* **41**, 415–417 (2018).
- ⁵⁸I. Tal, S. Neymotin, S. Bickel, P. Lakatos, and C. E. Schroeder, “Oscillatory bursting as a mechanism for temporal coupling and information coding,” *Front Comput Neurosci* **14**, 82 (2020).
- ⁵⁹R. Schmidt, J. Rose, and V. Muralidharan, “Transient oscillations as computations for cognition: Analysis, modeling and function,” *Curr Opin Neurobiol.* **83**, 102796 (2023).
- ⁶⁰A. A. Costa, L. Brochini, and O. Kinouchi, “Self-organized supercriticality and oscillations in networks of stochastic spiking neurons,” *Entropy* **19**, 399 (2017).
- ⁶¹K. Kaneko, “Relevance of dynamic clustering to biological networks,” *Physica D* **75**, 55–73 (1994).
- ⁶²K. Kaneko, *Theory and Applications of Coupled Map Lattices* (Wiley, 1993).
- ⁶³V. Hernandez-Urbina and J. M. Herrmann, “Self-organized criticality via retro-synaptic signals,” *Front. Phys.* **4**, 54 (2017).
- ⁶⁴R. Dickman, M. A. Muñoz, A. Vespignani, and S. Zapperi, “Paths to self-organized criticality,” *Braz. J. Phys.* **30**, 27–41 (2000).
- ⁶⁵P. Bak, C. Tang, and K. Wiesenfeld, “Self-organized criticality: An explanation of the $1/f$ noise,” *Phys. Rev. Lett.* **59**, 381 (1987).
- ⁶⁶P. Jiruska, M. De Curtis, J. G. Jefferys, C. A. Schevon, S. J. Schiff, and K. Schindler, “Synchronization and desynchronization in epilepsy: controversies and hypotheses,” *J Physiol.* **591**, 787–797 (2013).
- ⁶⁷B. C. Bernhardt, S. Hong, A. Bernasconi, and N. Bernasconi, “Imaging structural and functional brain networks in temporal lobe epilepsy,” *Front Hum Neurosci.* **7**, 624 (2013).
- ⁶⁸M. Girardi-Schappo, F. Fadaie, H. M. Lee, B. Caldaïrou, V. Sziklas, J. Crane, B. C. Bernhardt, A. Bernasconi, and N. Bernasconi, “Altered communication dynamics reflect cognitive deficits in temporal lobe epilepsy,” *Epilepsia* **62**, 1022–1033 (2021).
- ⁶⁹C. Meisel, A. Storch, S. Hallmeyer-Elgner, E. Bullmore, and T. Gross, “Failure of adaptive self-organized criticality during epileptic seizure attacks,” *PLoS Comput. Biol.* **8**, e1002312 (2012).
- ⁷⁰C. Meisel, “Antiepileptic drugs induce subcritical dynamics in human cortical networks,” *Proc. Nat. Acad. Sci. USA* **117**, 11118–11125 (2020).
- ⁷¹M. I. Maturana, C. Meisel, K. Dell, P. J. Karoly, W. D’Souza, D. B. Grayden, A. N. Burkitt, P. Jiruska, J. Kudlacek, J. Hlinka, *et al.*, “Critical slowing down as a biomarker for seizure susceptibility,” *Nat Commun.* **11**, 2172 (2020).
- ⁷²J. Žiburkus, J. R. Cressman, and S. J. Schiff, “Seizures as imbalanced up states: excitatory and inhibitory conductances during seizure-like events,” *J. Neurophysiol.* **109**, 1296–1306 (2013).
- ⁷³K. Chen, I. Aradi, N. Thon, M. Eghbal-Ahmadi, T. Z. Baram, and I. Soltesz, “Persistently modified h-channels after complex febrile seizures convert the seizure-induced enhancement of inhibition to hyperexcitability,” *Nat Med* **7**, 331–337 (2001).
- ⁷⁴D. E. Naylor, “Glutamate and gaba in the balance: Convergent pathways sustain seizures during status epilepticus,” *Epilepsia* **51**, 106–109 (2010).
- ⁷⁵D. Kasteleijn-Nolst Trenité, G. Rubboli, E. Hirsch, A. Martins da Silva, S. Seri, A. Wilkins, J. Parra, A. Covanis, M. Elia, G. Capovilla, U. Stephani, and G. Harding, “Methodology of photic stimulation revisited: updated european algorithm for visual stimulation in the EEG laboratory,” *Epilepsia* **53**, 16–24 (2011).
- ⁷⁶D. Hermes, D. G. A. Kasteleijn-Nolst Trenité, and J. Winawer, “Gamma oscillations and photosensitive epilepsy,” *Curr Biol* **27**, R336–R338 (2017).
- ⁷⁷C. J. Honey and T. Valiante, “Neuroscience: When a single image can cause a seizure,” *Curr Biol* **27**, R394–R397 (2017).
- ⁷⁸E. Sayari, A. M. Batista, E. C. Gabrick, K. C. Iarosz, M. Hansen, J. D. Szezech Jr, and F. S. Borges, “Dynamics of a perturbed random neuronal network with burst-timing-dependent plasticity,” *Eur Phys J Spec Top* **231**, 4049–4056 (2022).

- ⁷⁹B. Boaretto, R. Budzinski, T. Prado, and S. Lopes, “Mechanism for explosive synchronization of neural networks,” *Phys Rev E* **100**, 052301 (2019).
- ⁸⁰D. G. Clark and L. F. Abbott, “Theory of coupled neuronal-synaptic dynamics,” *Phys. Rev. X* **14**, 021001 (2024).
- ⁸¹H. Sompolinsky, A. Crisanti, and H. J. Sommers, “Chaos in random neural networks,” *Phys. Rev. Lett.* **61**, 259–262 (1988).
- ⁸²M. Rosenblum and A. Pikovsky, “Delayed feedback control of collective synchrony: An approach to suppression of pathological brain rhythms,” *Phys. Rev. E* **70**, 041904 (2004).
- ⁸³E. L. Lameu, F. S. Borges, R. R. Borges, K. C. Iarosz, I. L. Caldas, A. M. Batista, R. L. Viana, and J. Kurths, “Suppression of phase synchronisation in network based on cat’s brain,” *Chaos* . **26** (2016).
- ⁸⁴M. Mugnaine, A. S. Reis, F. S. Borges, R. R. Borges, F. A. Ferrari, K. C. Iarosz, I. L. Caldas, E. L. Lameu, R. L. Viana, J. D. Szezech, *et al.*, “Delayed feedback control of phase synchronisation in a neuronal network model,” *Eur Phys J Spec Top* **227**, 1151–1160 (2018).
- ⁸⁵A. S. Reis, K. C. Iarosz, F. A. Ferrari, I. L. Caldas, A. M. Batista, and R. L. Viana, “Bursting synchronization in neuronal assemblies of scale-free networks,” *Chaos Solitons Fractals* **142**, 110395 (2021).

Appendix A: Supplementary Information

This document contains extra figures and supporting information about the methods applied in the manuscript:

- We display the interspike interval distributions and power spectra of a single randomly selected neuron connected to the all-to-all network at and around the synchronization phase transition.
- We also explain in details the fitting of the damping time scale of the reverberating activity around the critical point.

Appendix B: The isolated neuron

Label	K	T	δ_i	u	ε	H	$I_i(t)$
S1	0.6	0.35	0.006	0.004	-0.98	-0.5	0
S2	0.6	0.35	0.006	0.004	-0.98	-0.2	-0.06
CS	0.6	0.35	0.006	0.004	-0.98	-0.95	0
B1	0.6	0.35	0.006	0.004	-0.98	-0.8	0
B2	0.7	0.5	0.008	0.004	-0.98	-0.9	0
B3	0.8	0.6	0.006	0.004	-0.99	-0.8	0

TABLE S1: Parameters for the attractors in Fig. 1 of the main text.

Appendix C: Microscopic activity characterization

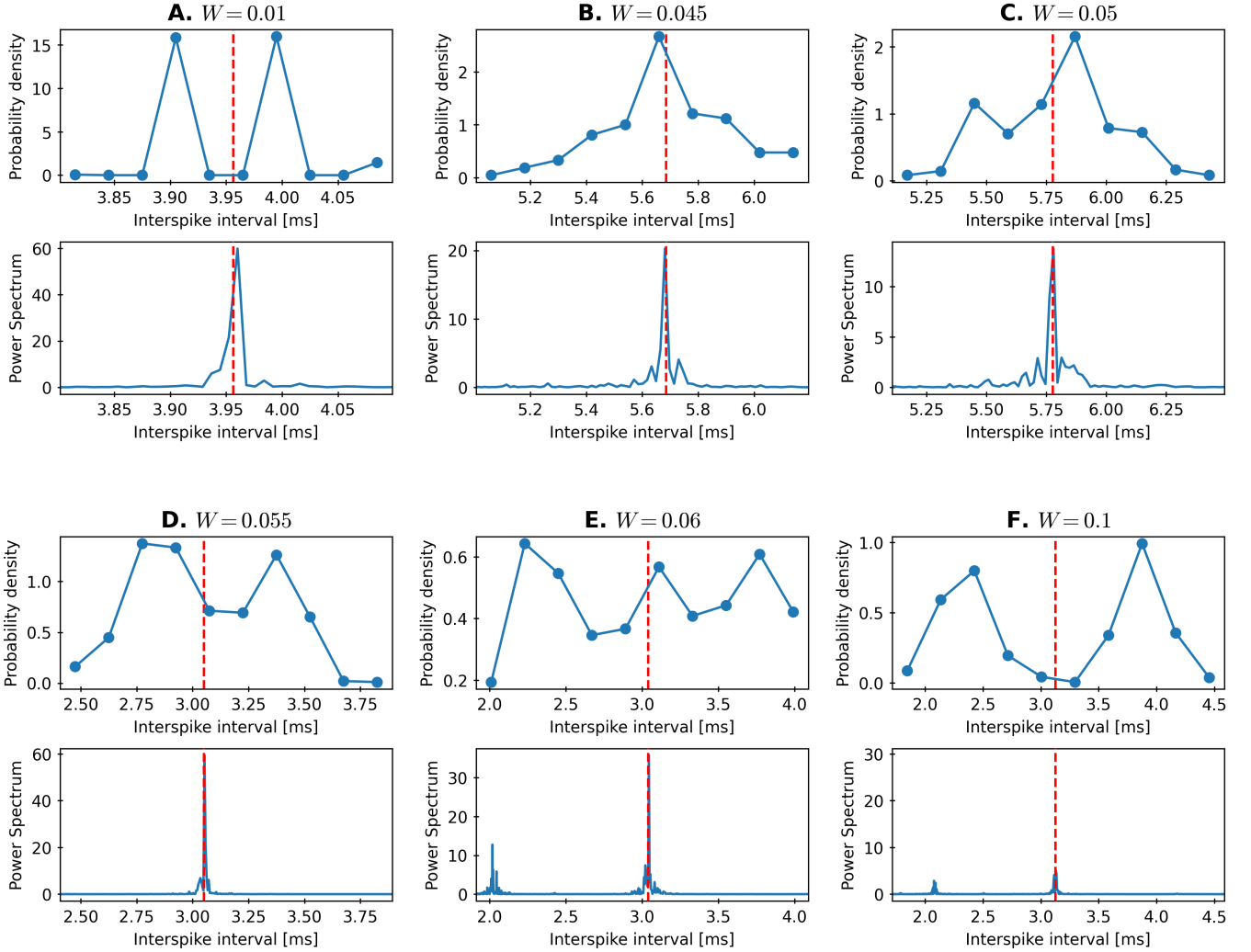


FIG. S1: Interspike interval of a neuron inside the network. A network of $N = 1000$ neurons is simulated for each W around the synchronization phase transition, and we characterize the activity of a single neuron within it. The interspike interval (ISI) distributions are broad and bimodal in both asynchronous and synchronous phases, although around the transition range ($0.045 \lesssim W \lesssim 0.05$) it becomes unimodal, assuming $W_c \approx 0.045$ (see the main text). Legend: $- - - \langle ISI \rangle$. Notice that $\langle ISI \rangle$ peaks along the transition range of W . It goes from $\langle ISI \rangle \approx 4$ ms for $W < W_c$, to $\langle ISI \rangle \approx 5.7$ ms at $W \approx W_c$, and then returns to $\langle ISI \rangle \approx 3$ ms for $W > W_c$. **A.** $W = 0.01$. **B.** $W = 0.045$. **C.** $W = 0.05$. **D.** $W = 0.055$. **E.** $W = 0.06$. **F.** $W = 0.1$. Parameters: $K = 0.6$, $T = 0.35$, $H = -0.2$, $\delta = 0.006$, $\Delta = 0.003$, $u = 0.004$, $\varepsilon = -0.98$.

Appendix D: Fitting the damping of the firing rate near the critical point

The firing rate of the network $\rho[t]$ is simply the average count of spikes per time step,

$$\rho[t] = \frac{1}{N} \sum_{i=1}^N S_i[t], \quad (\text{D1})$$

where $S_i[t] = 1$ if a spike happened at time t ($S_i[t] = 0$ otherwise). See the manuscript for the spike detection condition. We simulate the network until it reaches the stationary state, then continue in the stationary state for 1000 time steps (100 ms) before injecting the stimulus at $t_0 = 100$ ms. The time average $\langle \rho \rangle$ is taken over the pre-stimulus stationary state, $t < t_0$. The difference $\rho - \langle \rho \rangle$ is the detrended firing rate signal. From the observation of this signal, we assume that it can be written as the following function of the delay $\Delta t = t - t_0 > 0$

$$(\rho - \langle \rho \rangle)[\Delta t] = A[\Delta t]C[\Delta t],$$

where $A[\Delta t]$ is the time-dependent amplitude of the large oscillations $C[\Delta t]$.

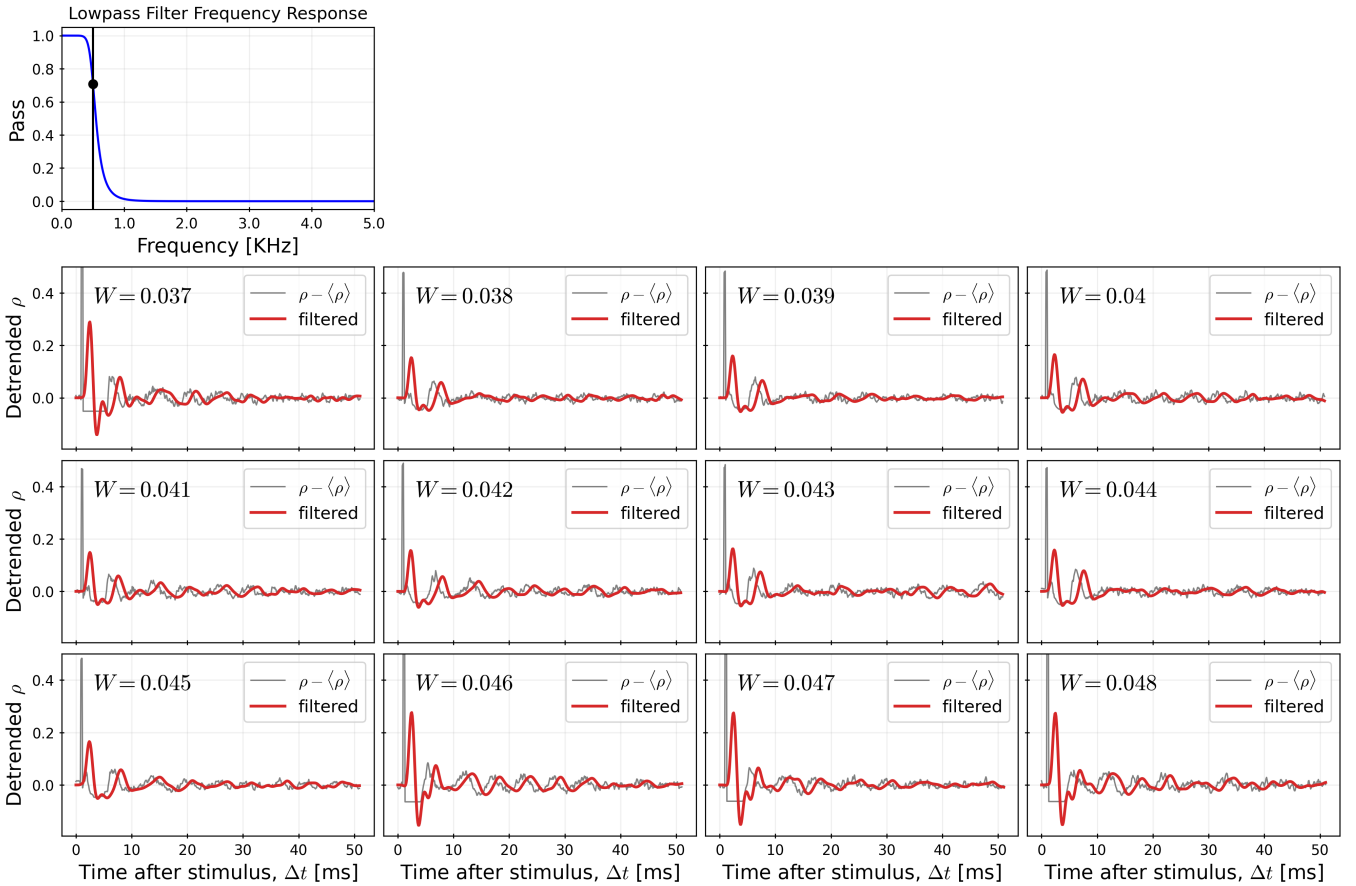


FIG. S2: Firing rate low-pass filter. **Top.** Filter response function showing a smooth cutoff of frequencies at 500 KHz. This filter is applied to the post-stimulus detrended firing rate oscillations of the network to produce a clean decay of the larger (and slower) oscillations. **Other panels.** Raw and filtered detrended firing rate $\rho - \langle \rho \rangle$ as a function of the delay after stimulus Δt . The filtered signal is slightly delayed, but its amplitude and damping match the noisy oscillations. The initial raw spike in the raw rate is the network response during the stimulus. W as given in the panels. Parameters: $N = 1000$, $K = 0.6$, $T = 0.35$, $H = -0.2$, $\delta = 0.006$, $\Delta = 0.003$, $u = 0.004$, $\varepsilon = -0.98$.

Now we describe the procedure to fit the amplitude A . This is applied independently to the detrended firing rate data of the simulated network for each W . First, we need to eliminate fast stochastic fluctuations from the detrended firing rate. Thus, we define a standard low-pass filter $F(u)$ with a soft threshold at 500 KHz (Fig. S2), and $u = (\rho - \langle \rho \rangle) \Delta t$ is the function of time to be filtered. We take the absolute value of the filtered signal $|F(\rho - \langle \rho \rangle)|$ in order to convert the wave valleys into peaks. We select peaks with prominence greater than 0.002 (in firing rate units, Fig. S3) and use them to fit the amplitude damping function:

$$A[\Delta t] = B\Delta t^{-\alpha} \exp(-\Delta t/\tau_A). \quad (\text{D2})$$

B is just a fitting constant, τ_A is the characteristic time of the damping during the post-stimulus delay Δt . α is a fixed parameter.

We sweep α over the range $[0.1; 0.8]$, and then for each α we perform a non-linear least squares fit of Eq (D2) to the amplitude peaks data and obtain $B(\alpha)$ and $\tau_A(\alpha)$ as functions of α . The statistical error E_{τ_A} of the fitted τ_A is also a function of α . We minimize E_{τ_A} to obtain the best fit:

$$\alpha_{\text{best}} = \underset{\alpha}{\text{argmin}}[E_{\tau_A}(\alpha)], \quad (\text{D3})$$

yielding $\tau_{A,\text{best}} = \tau_A(\alpha_{\text{best}})$. $\tau_{A,\text{best}}$ is the value shown in the panels of Fig. S3.

Since this is done independently for each W , the best fit values $\tau_{A,\text{best}}$ and α_{best} are functions of W (shown in Fig. 5C of the main text without the “best” subscript for clarity). To confirm the optimization of τ_A , we can replace α in Eq. (D2) by its average best value $\alpha = \bar{\alpha}_{\text{best}} = 0.20 \pm 0.05$, and again run the fit of τ_A and B . This results in the same behavior for τ_A as a function of W ; *i.e.*, τ_A is optimized at $W = 0.043$.

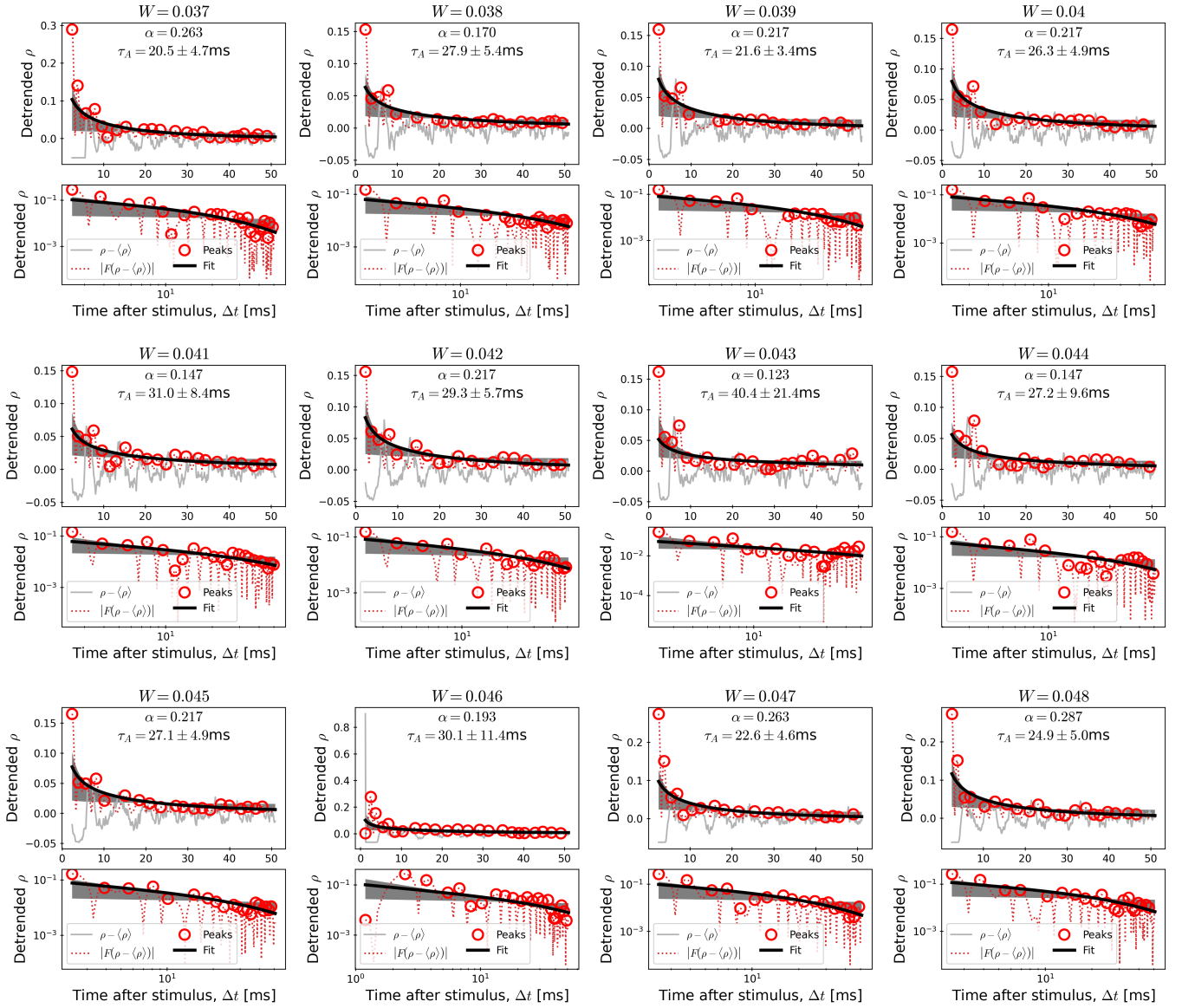


FIG. S3: Fitting the amplitude of the large and slow oscillations. The panels are presented in doubles (top and bottom of each of the three rows): for each W , the same data are shown on a linear scale (top of the row) and on a log-log scale (bottom of the row). We extracted the peaks of the absolute value of the filtered detrended firing rates, $|F(\rho - \langle \rho \rangle)|$, that had prominence greater than 0.002 (firing rate units) – shown in circles. We fitted Eq. (D2) for multiple α (remained fixed during fitting) to obtain the time scale τ_A of the damping. We show the α that minimized the error of τ_A (bold black line). Gray shading: Fit error range. W as given in the panels. Parameters: $N = 1000$, $K = 0.6$, $T = 0.35$, $H = -0.2$, $\delta = 0.006$, $\Delta = 0.003$, $u = 0.004$, $\varepsilon = -0.98$.